Microsystem Technologies
https://doi.org/10.1007/s00542-024-05759-z

TECHNICAL PAPER

DFT study of $MoSe_2$ monolayers for cohesive adsorption of harmful gases CO, CO_2, SO_2, and NF_3

Suman Sarkar[1] · Papiya Debnath[2] · Debashis De[3] · Manash Chanda[4]

Received: 2 May 2024 / Accepted: 26 August 2024

Abstract
According to the World Health Organization, contact with atmospheric airborne pollutants (CO, CO_2, SO_2, and NF_3) causes 4.2 million deaths annually. Globally, there is a well-established demand for highly sensitive, inexpensive, tiny, and energy-efficient gas sensors that are able to recognize and steer clear of high pollution hotspots. Density functional theory (DFT) is utilized to analyze the electronic properties of CO, CO_2, SO_2, and NF_3 gases in the $MoSe_2$ monolayer for gas sensing mechanism. On $MoSe_2$, calculations and discussions are made on the adsorption energies and configurations that are most stable. A detailed analysis is conducted on the adsorption distance (d (Å)), charge transfer (Q_T), adsorption energy (E_{ads}), band gap (E_g), density of states (DOS), electron difference density (EDD), and Recovery time (τ). The outcomes attained demonstrate that the adsorption of CO, CO_2, SO_2, and NF_3 gases significantly alters the electrical characteristics as well as the adsorption of $MoSe_2$ monolayer. However, in comparison to CO, CO_2, and SO_2, the $MoSe_2$ monolayer system shows larger adsorption energy towards NF_3 and a higher sensitivity. The transport characteristics employing the non-equilibrium Green's function (NEGF) method validate the efficiency of the $MoSe_2$ monolayer in terms of considerable current–voltage (I–V) response for enhanced CO, CO_2, SO_2, and NF_3 gas sensing. Compared to CO, CO_2, and SO_2, $MoSe_2$ has a much higher sensitivity to NF_3.

1 Introduction

Among the greatest dangers to human health in contemporary times is environmental air pollution. The World Health Organization (WHO) claimed in 2019 that 91% of people worldwide live in areas where air pollution levels are higher than recommended. Because fossil fuels are so economical, developing nations are still hesitant to limit their usage of them. Gases including nitrogen trifluoride (NF_3), carbon monoxide (CO), carbon dioxide (CO_2), and sulfur dioxide (SO_2) are examples of harmful gases, that have emerged as a troubling problem. For example, the poisonous, odorless, tasteless, and colorless CO gas is produced when fuels like natural gas and oil burn partially (Yogi and Jaiswal 2019). The ability of CO to bind with hemoglobin is now known to be essential to its toxicity mechanism, which results in a hypoxic environment inside cells (Gorman et al. 2003). The principal greenhouse gas responsible for the phenomenon of global warming is carbon dioxide (CO_2) (Yamakasi 2003). Moreover, one of the primary air pollutants created largely by industrial processes as well as the burning of coal and oil is SO_2, a colorless, corrosive, and powerful excitant odor (Yang et al. 2016). When SO_2 is dissolved in water, it generates sulfuric acid, which has a major negative impact on human skin and the mucous membranes of the eyes and nose (Yang et al. 2016). Global warming might be triggered 16,600 times more often by nitrogen trifluoride (NF_3) than by carbon dioxide (CO_2). Its atmospheric lifespan is

✉ Manash Chanda
manash@msit.edu.in

Suman Sarkar
suman.sarkar@iem.edu.in

Papiya Debnath
papiya.debnath@tict.edu.in

Debashis De
dr.debashis.de@gmail.com

[1] Electrical and Electronics Engineering Department, Institute of Engineering and Management, University of Engineering and Management, Kolkata, India

[2] Department of BSH, TINT New Town, Kolkata, India

[3] Computer Science and Engineering Department, Maulana Abul Kalam Azad University of Technology, Kalyani, India

[4] Electronics and Communication Engineering Department, Meghnad Saha Institute of Technology, Kolkata, India

Published online: 07 September 2024

740 years (Tsai 2008; Lu et al. 2017). It's important to note that NF_3 is one of the fluorine sources that the electronics sector uses extensively (Flamm 1993). Each of these pollutants has suggested exposure limits, and when they are surpassed, they can have a negative effect on the environment in a few ways, including eutrophication (the disturbance of ecosystems owing to an abundance of nutrients), acidification (acid rain), and global warming. Since its start, the study of gas sensing has been primarily concerned with contaminated or poisonous gas sensing, industrial monitoring, agricultural output, and health diagnostics (Chen et al. 2013). The ability to detect hazardous gases is crucial because it supports both the protection of human health and the monitoring and management of environmental pollution (Tit et al. 2017; Zhao et al. 2020).

2-D nanomaterials have attracted a lot of attention for potential new gas sensing applications since the successful experiment synthesis of graphene (Geim 2007; Zhang et al. 2016). The primary benefits of nanostructures for detecting gases are their larger surface-active site, large surface-to-volume ratio, small size and dimensions, and large specific surface area. The use of nanoparticles for gas removal and monitoring is becoming more and more necessary. The use of resistive sensors is important in environmental monitoring because they use surface coatings to increase surface contact-mediated electron transit among the gases and the substrate (Pearton et al. 2010) and to use electrical resistance adjustment to measure gas concentrations (Zhang et al. 2021). Growing gas-sensitive materials that work at room temperature is crucial. It is essential to growing gas-sensitive materials that can function at ambient temperature. However, due to the advantages of low cost, micro miniaturization, superior physicochemical stability, and remarkable detecting characteristics, sensors for gases made from nanosized semiconductors are becoming increasingly common. The study thus focused on contemporary nanoscale semiconductor-based gas detectors (Zhang et al. 2017). Despite graphene-based chemical sensors receiving much attention due to their superior gas-sensing capabilities, poor switching characteristics are caused by graphene's zero-band gap (Geim 2007). A variety of materials in two dimensions, including III–IV compounds, V group monolayers, and transition metal dichalcogenides (TMDs), have recently been shown to have strong interactions with gas molecules and should possess strong electron mobility and good chemical reactivity (Cui et al. 2019a; Zhang et al. 2018).

The novelty lies in the specific combination of material ($MoSe_2$), the theoretical approach (DFT), and the focus on multiple harmful gases, all of which contribute to advancing knowledge in the field of 2-D materials and their applications in environmental technology (Zhao et al. 2017; Shen et al. , 2022; Kadioglu et al. 2017). The study focuses on the unique properties of molybdenum diselenide ($MoSe_2$) monolayers, which are a less explored material compared to more common 2-D materials like graphene or MoS_2, WS_2, WSe_2 etc. (Zhao et al. 2017; Shen et al. , 2022; Kadioglu et al. 2017). The paper examines the adsorption behavior of multiple harmful gases (CO, CO_2, SO_2, and NF_3), providing a broad spectrum of data. This comprehensive analysis could reveal differential adsorption capacities and mechanisms for each gas, contributing to a deeper understanding of the material's selectivity and efficiency. By exploring the adsorption of environmentally harmful gases, the research has significant implications for pollution control and environmental protection. The findings could lead to the development of effective gas sensors or filters based on MoSe2 monolayers. Based on the first principal simulations, it was determined that the BN bilayer is a potential optical sensor for SO_2, CO_2, and NO_2. Its adsorption properties for CO_2, SO_2, and NO_2 were calculated (Hussein et al. 2023). By using the first principles to analyze the electrical behavior of (CO, CO_2, SO_2) gases adsorbed on the armchair graphene nanoribbon monolayer (Salih and Ayes 2020). By applying the first principles to the electrical behavior of SO_2, CO_2 gases adsorbed on the Cu-doped WSe_2 monolayer found that CO_2 and H_2S adsorption performed better (Cui et al. 2022).

We describe the design and theoretical discussion of a 2-D $MoSe_2$ monolayer-based ecologically harmful gas sensor, applying the first-principles density functional theory (DFT). High chemical stability, quick reaction times, and sensitivity are necessary for an outstanding gas sensor (Sajjad and Feng 2014). A novel approach to creating a new gas sensor could be offered by the 2-D $MoSe_2$ monolayer. The Band structure, density of states (DOS), recovery time, and charge transfer (Q_T) were also computed in order to determine the differences between the pure 2-D $MoSe_2$ monolayer and the gas molecules adsorbed $MoSe_2$ nanosheet, wherein the environmentally hazardous CO, CO_2, SO_2, and NF_3 molecules are taken into account. The Non-Equilibrium Green's Function (NEGF) technique was utilized to determine the current–voltage (I–V) characteristic to validate the sensing application in a realistic scenario.

2 Theory and method of simulations

A $MoSe_2$ supercell 6×6 with ambient gas molecules adsorbed onto it served as the basis for the system. Exchange–correlation factions were generated in $DMol^3$'s (Diederich et al. 1992) calculation process using the PBE i.e., Perdew–Burke–Ernzerhof (Delley 1990; Cui et al. 2019b) algorithm within a general gradient approximation

i.e., GGA. The grid-mesh cutoff is set to 500 eV for $MoSe_2$ nanosheet structural optimization. Using a Methfessel-Paxton smearing of 0.01 Ry and a $1 \times 4 \times 4$ Monkhorst–Pack k-point grid, the Brillouin zone was sampled. All atomic structures were relaxed until the Hellmann–Feynman force as well as total energy reached 1.0×10^{-5} eV and 0.06 eV/Å, respectively (Becke 1993). $MoSe_2$ nanosheets were optimized using the double-zeta polarization (DZP) and conjugated gradient (CG) algorithms. The weak van der Waal contact has been considered between the 2-D single-layer nanoribbon and gas molecule and is done using Grimme's DFT-D2 method (Grimme 2006; Sarkar et al. 2022). To estimate the numerous qualities that the GGA-PBE functional is unable to estimate, the Grimme dispersion term is utilized to account for extended interactions. We determined the adsorption energy (E_{ads}) of adsorbed systems, which was specified as follows, to evaluate the gas-molecule interaction with the surface of the adsorption sheet.

The capacity for adsorption was determined by putting a molecule of gas on top of a 2-D $MoSe_2$ monolayer and letting it move in three dimensions while the structure was optimized. In order to evaluate the interactions among gas molecules and the adsorption 2-D single layer (Sarkar et al. 2023), we computed the energy needed for the adsorption of the adsorbed configuration, which was given as follows.

We determined the adsorption energy (E_{ads}) of adsorbed systems, which was specified as follows, to assess the interplay between gas molecules as well as the adsorption sheet surface (Sarkar et al. 2023).

$$E_{ads} = E_{MoSe_2@GAS} - (E_{MoSe_2} + E_{GAS}) \tag{1}$$

where E_{MoSe_2} is the $MoSe_2$ energy, E_{GAS} is the CO, CO_2, SO_2, and NF_3 gases energy, and $E_{MoSe_2@GAS}$ represents the overall energy of the system that has been adsorbed with $MoSe_2$. The calculations for all energies used optimized atomic structures. Adsorption energy plays a crucial role in determining whether adsorption is exothermic or endothermic. The negative value of adsorption energy indicates favorable adsorption i.e., exothermic, and the positive value of adsorption energy indicates unfavorable adsorption i.e., endothermic.

The difference between the highest conduction band and the bottom valence band can be used to compute the band gap.

$$E_g = V_{(V.B)} - V_{(C.B)} \tag{2}$$

The Mulliken population equation was utilized to compute the amount of the transferred charges of the above-mentioned gases (Bo et al. 2019; Mulliken 1955):

$$Q_T = Q_{ads} - Q_{iso} \tag{3}$$

where the gas's charge transfer is denoted by Q_T, Q_{ads}, and Q_{iso}, and the Mulliken charges of the gas before and after adsorption, respectively. $Q_T < 0$ indicates gas electron loss.

The NEGF technique was used to do the electrical transport calculations (30). The basis sets that are double-ζ polarized (DZP) and have an energy cut-off of 250 Ry were employed in the computations. Regarding the electrode and transportation computations, Monkhorst–Pack k-point grids of $1 \times 1 \times 80$ were utilized. The Landauer-Buttiker formulation defines the connection between current and voltage throughout the system of atoms scale (Sarkar et al. 2023).

$$I(V_{bias}) = G_0 \int \Im(E, V_{bias})[f(E - \mu_L) - f(E - \mu_R)]dE \tag{4}$$

where V_{bias} and $f_{L/R}(E)$ stand for the applied bias voltage and the left/right electrode's Fermi–Dirac distribution functions, respectively, and L/R represents the electrodes' chemical potential $\mu_{L/R}$. The probability of electrons incidental at energy (E) under potential bias (V_{bias}) is represented by $\Im(E, V_{bias})$. $G_0 = 2e^2/h$ represents the quantum conductance (Fig. 1).

3 Result and discussion

3.1 The properties of structure

Figure 2a depicts the $MoSe_2$ unit cell, which has three atoms total (Se: 2 and Mo: 1) arranged in the regular hexagonal lattice, representing the equilibrium structure of the monolayer $MoSe_2$. Mo–Se and Se–Se bond lengths were determined to be 2.31 Å and 3.288 Å. The layered hexagonal unit cell of $MoSe_2$ has a lattice constant of $|\alpha| =$ 3.319 Å. As a result, the monolayer of $MoSe_2$ has a significantly bigger atomic structure than WS_2 and MoS_2-TMDs due to Se's high atomic radius. The lattice constant and length of bond found for the 2-D $MoSe_2$ monolayer in the present investigation agree with recently published studies (Kang et al. 2013) and experimental work (Nagarajan and Chandiramouli 2017). $MoSe_2$ monolayer is made up of three layers of atoms, with Se atoms in the upper and lower layers and Mo atoms in the middle layer. Before analyzing the adsorption behavior on the surface of a single-layer $MoSe_2$, we computed the optimized geometry of the $MoSe_2$ monolayer $1 \times 4 \times 4$ supercell, as illustrated in Fig. 2a.

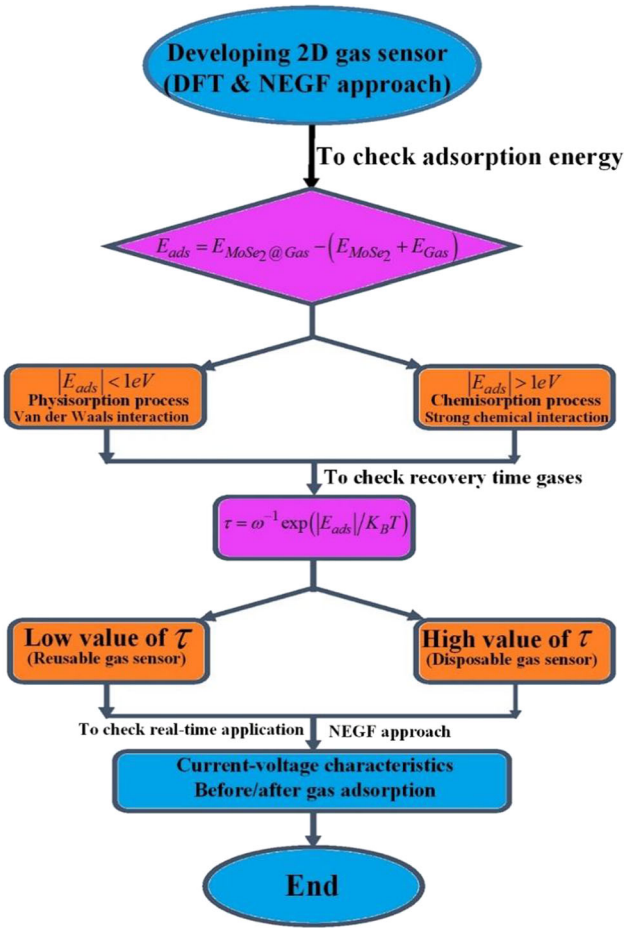

Fig.1 Flow chart of the simulation framework

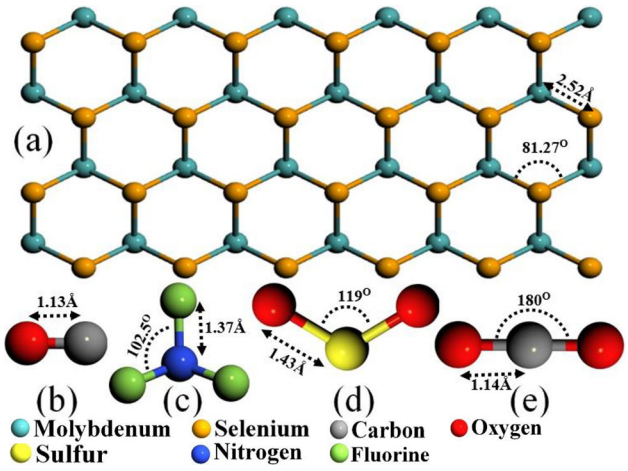

Fig. 2 The geometry of **a** pristine $MoSe_2$ monolayer, **b** CO, **c** NF_3, **d** SO_2, **e** CO_2

4 CO molecules adsorption on $MoSe_2$ nanosheet

The adsorption of CO has also been shown in Fig. 3a, c. The CO molecule has a linear structure with a 1.13Å C–O bond. Additionally, oxygen in the carbon monoxide molecule hybridizes its orbitals to create three sp hybrid orbitals. O atom of CO molecule adsorbed on Se of $MoSe_2$ monolayer. The bond length between Se of $MoSe_2$ and O of CO molecules is found 2.05 Å. The adsorption energy of the system is found − 0.93 eV. The calculated charge transfer (Q_T) is − 0.03e, as shown in Table 1. The negative sign of the transfer of charges signifies that CO transfers the charge to the $MoSe_2$. The electron difference density (EDD) plot is shown in Fig. 4a, c.

$$Mo_{24}Se_{48} + CO \rightarrow Mo_{24}Se_{48}@CO + E_{ad}, \ (E_{ad} = -0.93 \text{ eV}) \quad (5)$$

5 CO_2 molecules adsorption on $MoSe_2$ nanosheet

The adsorption of CO_2 has also been illustrated in Fig. 3b, d. The CO_2 molecule has a linear structure with a 1.14 Å C–O bond. Additionally, oxygen in the carbon dioxide molecule hybridizes its orbitals to create three sp^2 hybrid orbitals. After adsorption of CO_2 on $MoSe_2$ monolayer it is found that the calculated distance between the C of CO_2 and Se of $MoSe_2$ is 1.83 Å. The calculated adsorption energies are − 0.8 eV for CO_2. The charge transfer from $MoSe_2$ to CO_2 gas molecule was 0.017e, the positive sign signifies that 0.017e charge from $MoSe_2$ to CO_2. The electron difference density (EDD) plot is shown in Fig. 4b, d.

$$Mo_{24}Se_{48} + CO_2 \rightarrow Mo_{24}Se_{48}@CO_2 + E_{ad}, \ (E_{ad} = -0.8 \text{ eV}) \quad (6)$$

6 SO_2 molecules adsorption on $MoSe_2$ nanosheet

The adsorption of SO_2 has also been illustrated in Fig. 3e, g. The SO_2 molecule has a linear structure with a 1.43Å S–O bond. Additionally, oxygen in the Sulfur dioxide molecule hybridizes its orbitals to create three sp^2 hybrid orbitals. In $MoSe_2@SO_2$ the bond length between Se of $MoSe_2$ and S of SO_2 is 1.54 Å. The adsorption energy of the system is − 0.54 eV, and the charge transfer from $MoSe_2$ to SO_2 gas molecule was 0.21e, the positive sign signifies

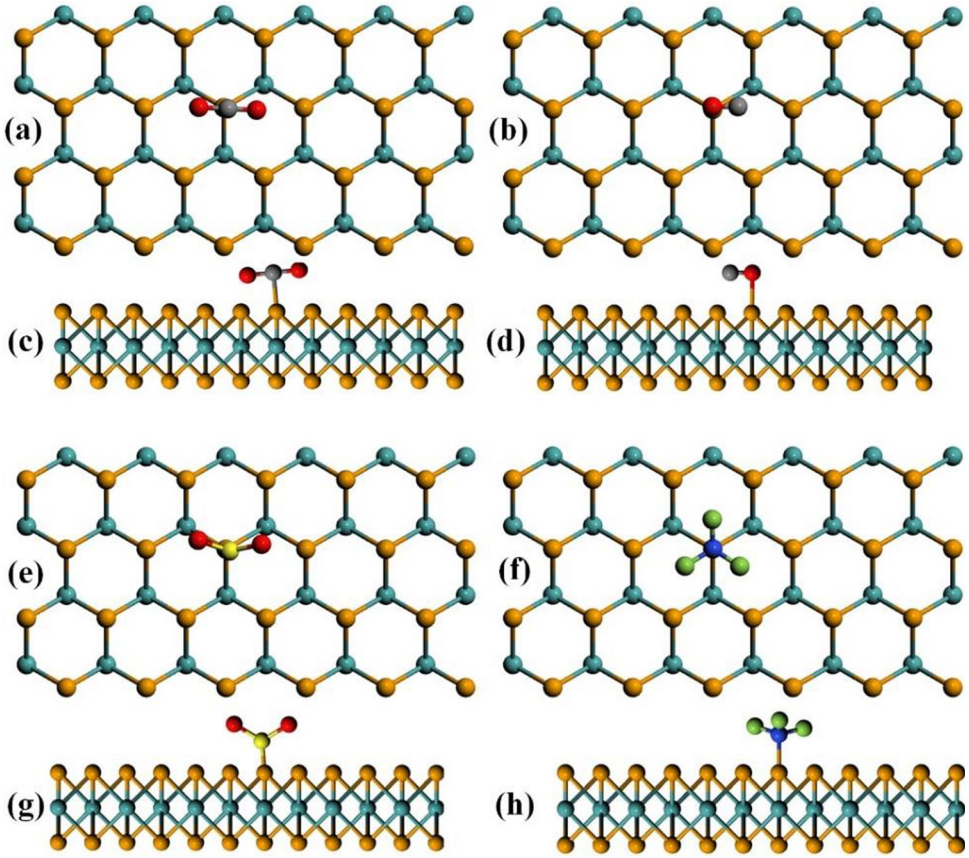

Fig. 3 The geometry of **a** top view of CO adsorbed $MoSe_2$ monolayer, **b** top view of CO_2 adsorbed $MoSe_2$ monolayer, **c** front view of CO adsorbed $MoSe_2$ monolayer, **d** front view of CO_2 adsorbed $MoSe_2$ monolayer, **e** top view of SO_2 adsorbed $MoSe_2$ monolayer, **f** top view of NF_3 adsorbed $MoSe_2$ monolayer, **g** front view of SO_2 adsorbed $MoSe_2$ monolayer, **h** front view of NF_3 adsorbed $MoSe_2$ monolayer

Table 1 Comparison study of adsorption parameters between CO, CO_2, SO_2, and NF_3 molecule and $MoSe_2$: E_{ads} for the adsorption energy, *d*, Q_T, Style, and E_g for distance, charge transfer, Type of the charge transfer, and Energy Band Gap

	Gas	E_{ads} (eV)	d (Å)	Q_T (e)	Style	E_g (eV)	References
BN bilayer	CO_2	− 0.3854	3.11 (N–C)	0.02	Donor	4.441	Hussein et al. (2023)
	SO_2	− 0.5322	3.04 (B-O)	0.03	Donor	1.876	
	NO_2	− 0.3255	2.86 (B-N)	0.01	Donor	2.471	
AGNR	CO	− 0.26	3.14	− 0.019	Acceptor	NR#	Salih and Ayes (2020)
	CO_2	− 0.145	3.25	− 0.009	Acceptor	NR#	
	SO_2	− 0.196	3.14	− 0.008	Acceptor	NR#	
WSe_2	SO_2	− 0.35	3.04	− 0.12	Acceptor	NR#	Cui et al. (2022)
	CO_2	0.19	3.4	− 0.01	Acceptor	NR#	
$MoSe_2$	CO	− 0.93	2.05 (Se-O)	− 0.002	Acceptor	1.39	Present study
	CO_2	− 0.8	1.83 (Se-C)	0.017	Donor	1.25	
	SO_2	− 0.54	1.54 (Se-S)	0.021	Donor	0.86	
	NF_3	− 0.5	1.48 (Se-N)	− 0.03	Acceptor	0.64	

N.B. Eg = 1.43 eV; NR# = Not reported

that $0.21e$ charge from $MoSe_2$ to SO_2. The electron difference density (EDD) plot is shown in Fig. 4e, g.

$$Mo_{24}Se_{48} + SO_2 \rightarrow Mo_{24}Se_{48}@SO_2 + E_{ad},\ (E_{ad} = -0.54eV) \quad (7)$$

7 NF_3 molecules adsorption on $MoSe_2$ nanosheet

The adsorption of NF_3 has also been shown in Fig. 3f, h. The NF_3 molecule has a linear structure with a 1.37 Å N–F bond. Additionally, oxygen in the Nitrogen trifluoride molecule hybridizes its orbitals to create three sp^3 hybrid orbitals. In $MoSe_2@NF_3$ the bond length between Se of

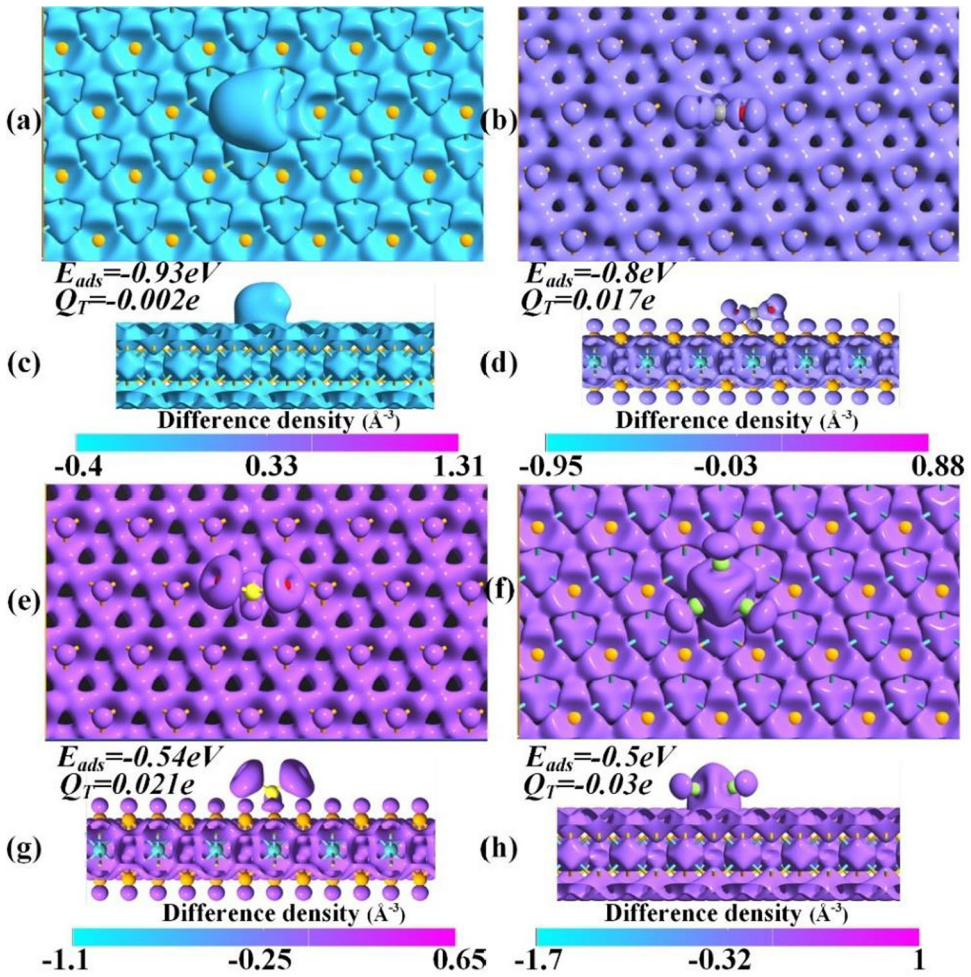

Fig. 4 The electron difference density (EDD) plot **a** top view of CO adsorbed $MoSe_2$ monolayer, **b** top view of CO_2 adsorbed $MoSe_2$ monolayer, **c** front view of CO adsorbed $MoSe_2$ monolayer, **d** front view of CO_2 adsorbed $MoSe_2$ monolayer, **e** top view of SO_2 adsorbed $MoSe_2$ monolayer, **f** Top view of NF_3 adsorbed $MoSe_2$ monolayer, **g** front view of SO_2 adsorbed $MoSe_2$ monolayer, **h** front view of NF_3 adsorbed $MoSe_2$ monolayer

$MoSe_2$ and N of NF_3 is 1.48 Å. The adsorption energy of the system is − 0.5 eV, the charge transfer from $MoSe_2$ to NF_3 gas molecule was $-0.03e$, and the negative sign signifies that $0.21e$ charge to $MoSe_2$ from SO_2. The electron difference density (EDD) plot is shown in Fig. 4f, h.

$$Mo_{24}Se_{48} + NF_3 \rightarrow Mo_{24}Se_{48}@NF_3 + E_{ad},\ (E_{ad} = -0.5eV) \quad (8)$$

8 Electronic properties of CO, CO_2, SO_2, and NF_3 adsorbed on $MoSe_2$ surface

Figure 5a, e illustrates how gas adsorption (CO, CO_2, SO_2, and NF_3) affects the band structure of pristine $MoSe_2$ systems. Notable changes in the band structure due to adsorption for both gases are shown in Fig. 5. Table 1 shows the observed changes for both pure $MoSe_2$ crystals. Our study shows that the band structure of $MoSe_2$ monolayer 1.43 eV which is very close to 1.55 eV reported in previous studies (Geim 2007) as mentioned in Table 1. After adsorption of CO on the $MoSe_2$ monolayer, the band gap is lowered to 1.39 eV, shown in Fig. 5b i.e., a fall of 5.6% can be noticed as compared to $MoSe_2$. After adsorption CO_2 on $MoSe_2$ monolayer addition of bands can be observed near the conduction and valance band close to Fermi level as illustrated in Fig. 5c. The reduced band gap is 1.25 eV, which is 12.6% lower as compared to $MoSe_2$. Hybridization and orbital overlaps are likely to blame for the bandgap's reduction. SO_2 adsorption causes the band gap of the $MoSe_2$ monolayer to drop to 0.86 eV, i.e., a 39.9% drop as compared to Pure $MoSe_2$ can be observed. Moreover, because both gases adsorb on virgin structures, new subbands form within the valence bands as well as conduction bands. Furthermore, $MoSe_2$ exhibits a significantly less band gap difference following NF_3 adsorption than other gases. The determined band gap is 0.64 eV which is 56% less as compared pristine $MoSe_2$ monolayer. The band gap's modifications after the adsorption of CO, CO_2, SO_2, and NF_3 gas molecules, as well as all the newly formed bands both above and below the Fermi level, indicate that the band structure analysis's conclusions may also be used to validate the sensing of CO, CO_2, SO_2, and NF_3 gas molecules. The changes observed in the density of

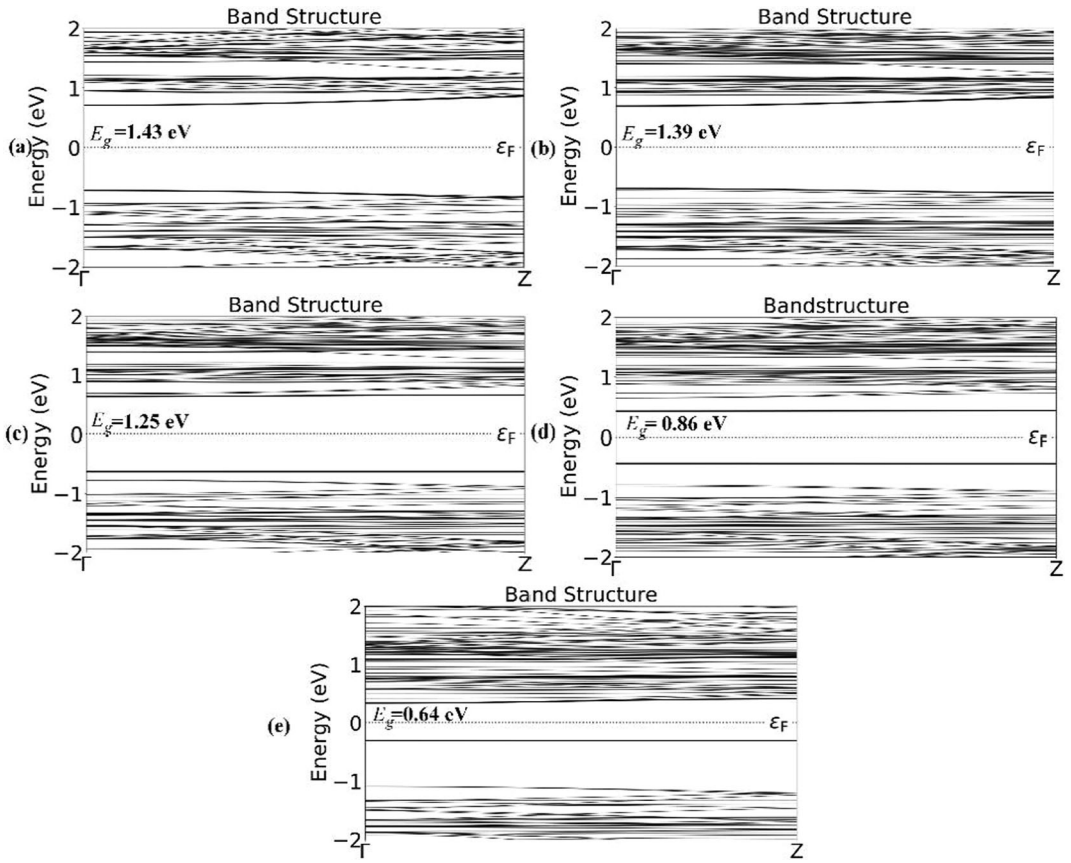

Fig. 5 Band structures of **a** 2-D pristine $MoSe_2$ monolayer, **b** CO adsorbed $MoSe_2$ monolayer, **c** CO_2 adsorbed $MoSe_2$ single layer, **d** SO_2 adsorbed $MoSe_2$ monolayer, **e** NF_3 adsorbed $MoSe_2$ single layer

states (DOS) after the adsorption of all the gases are explained by the formation of new subbands, as can be seen below.

The adsorption of both gases on pure $MoSe_2$ structures causes the DOS to be analyzed to study the electronic energy levels in the valance and conduction bands, as seen in Fig. 6a–e. The energy range of the systems taken from − 2 to 2 eV is displayed in Fig. 6. As seen in Fig. 6a, the DOS plot of the $MoSe_2$ monolayer. The DOS plot consists of the Total DOS of $MoSe_2$ monolayer, Mo, d orbital, and Se, p-orbital with similar peck position. The available energy states can be observed from − 0.72 to − 2 eV on the right side and 0.71–2 eV on the Fermi level's left side in the DOS plot. On the left side of the Fermi level, several peaks can be observed. The highest peak is present at 1 eV. Figure 6b shows that the adsorption on $MoSe_2$ monolayer introduces new energy levels at − 0.67 eV to − 0.72 eV and 0.68 eV to 0.71 eV within the conduction as well as valance bands, respectively, indicating a decrease in band gap energy. After adsorption peak present in the conduction band is also reduced. P-orbital of the O and C atoms present in the CO is responsible for the addition of new energy levels. The peaks of both sides of the Fermi level are influenced by the d-orbital of Mo. It's interesting to note that CO_2 will be adsorbed in a manner akin to CO adsorption when interacting with the $MoSe_2$ monolayer. The electronic structure presented in Fig. 6c indicates that the strong bonding between C–Se is correlated with the Mo d-, Se p-, C p- and O p-orbitals, respectively. As a result of CO_2 adsorption on the $MoSe_2$ monolayer new energy bands were added to both sides of the conduction from 0.58 to 0.71 eV and a valance band from − 0.62 to − 0.72 eV. Figure 6d represents the DOS plot of SO_2 adsorbed $MoSe_2$ monolayer. The primary cause of the alteration of the occupied states of DOS for pristine $MoSe_2$ systems is the newly occupied electronic states that come from SO_2 adsorption. d—Orbital of Mo in $MoSe_2$ and p—orbital O in SO_2 are responsible for additional energy states in valance and conduction band. At around 0.4 eV and − 0.4 eV an addition of energy states can be observed on both sides of the fermi level. DOS plot $MoSe_2$@NF_3 shown in Fig. 6e, the addition of a significant amount of energy states introduced because of the adsorption of NF_3 on $MoSe_2$. The energy states were observed near − 0.27 eV in the valance band and at 0.32 eV in the conduction band. P-orbital of N in NF_3 and d-orbital of Mo in $MoSe_2$

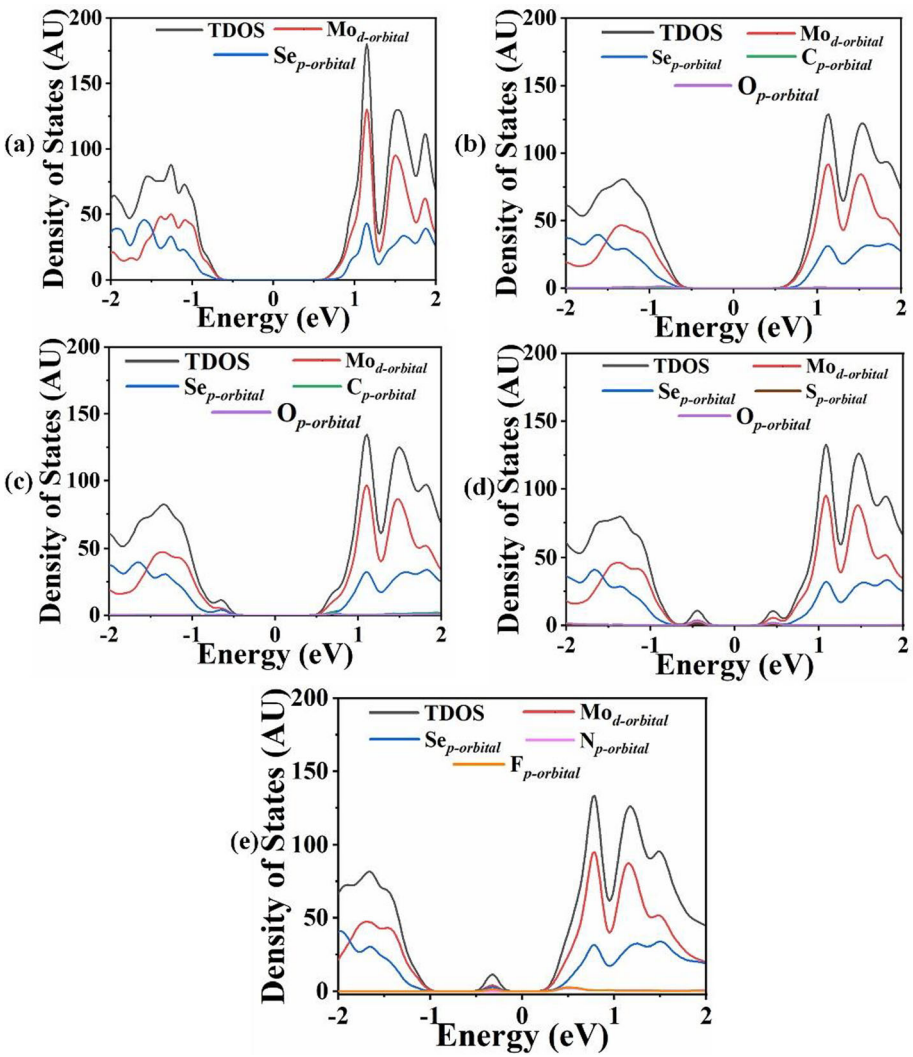

Fig. 6 DOS plot of **a** pristine 2-D $MoSe_2$ monolayer, **b** CO adsorbed $MoSe_2$ monolayer, **c** CO_2 adsorbed $MoSe_2$ monolayer, **d** SO_2 adsorbed $MoSe_2$ monolayer, **e** NF_3 adsorbed $MoSe_2$ monolayer

monolayer. Because it contains "chemisorption" occurrence, when it comes to identifying CO gas molecules, the $MoSe_2$ system is incredibly sensitive and selective. The chemisorption process has a significant impact on both bandgap narrowing and electrical structure.

9 Recovery property

A shorter span of recovery time might be advantageous for a gas sensor's reversibility. The sensor is heated to extreme temperatures to experimentally evaluate the recovery time; however, in principle, it is computed using the transition state theory, which establishes the connection between the recovery period and the adsorption energy. Thus, it is important to remember that in sensing applications, the recovery time is crucial. The Van't Hoff-Arrhenius expression (Demir and Fellah 2020) for the rate constant may be used to estimate the recovery time (τ). This can be done by using the definition that follows.

$$\tau = \frac{1}{\omega \exp\left(E_{ads}/K_B T\right)} \tag{8}$$

where it is typically believed that the attempt frequency (ω) is "a typical value" in the range of 10^{12}–10^{13} s^{-1} according to transition state theory, it is assumed to be 10^{12} s^{-1}, where T represents temperature, the Boltzmann constant is denoted by K_B $(8.318 \times 10^{-3}$ kJ/(mol K)) (Peng et al. 2004; Hoa et al. 2009). We take the value of E_{ads} to represent the potential barrier (E_a) of the process of desorption since desorption is thought of as the opposite of adsorption (Cui et al. 2019c; Sarkar et al. 2021). To completely comprehend the 2-D $MoSe_2$ monolayer desorption property, we considered the temperatures of 300 K, 400 K, and 500 K. The computed recovery time is presented in Fig. 5. Which illustrates how the recovery period may magnify an adsorption energy differential of less than

1 eV by many orders of magnitude. $MoSe_2$@CO has the longest recovery time i.e., 3422.8 s at the temperature of 300 K. The $MoSe_2$@NF_3 system has the quickest recovery time i.e., 0.23 ms. The recovery time of the adsorbed system can be arranged as follows $MoSe_2$@NF_3 < $MoSe_2$@SO_2 < $MoSe_2$@CO_2 < $MoSe_2$@CO. Recovery time also depends on temperature as illustrated in Fig. 5. As the temperature rises the recovery time decreases. Thus, the candidate materials with the right gas adsorption energy and quick response time should be chosen when other requirements are satisfied (Fig. 7).

10 Current–voltage

To evaluate the true implications of 2-D $MoSe_2$ monolayer for CO, CO_2, SO_2, and NF_3 gas sensor, it has to be investigated as a gas resistive sensor or field effect transistor (FET), where the main variable reacts to the resistance or threshold voltage. To test the 2-D $MoSe_2$ monolayer output with and without CO, CO_2, SO_2, and NF_3 gas molecules, we thus employed the NEGF technique to compute the transport properties for a wide spectrum of (voltage). A scattering zone was placed between the left as well as right electrodes, which were modeled using identical material. The hazardous gasses CO, CO_2, SO_2, and NF_3 are adsorbed in the scattering region, and the electrode is thought to be semi-infinite (Fig. 8).

In all critical computations, relaxed upper cell structures are used to analyze electronic transport characteristics. To draw similarities, the current (I)–voltage (V) characteristics without the gases were examined. A monolayer is used to adsorb the gas molecules CO, CO_2, SO_2, and NF_3. The induced current for NF_3 is more than that of any other molecule used here such as CO, CO_2, and SO_2 when

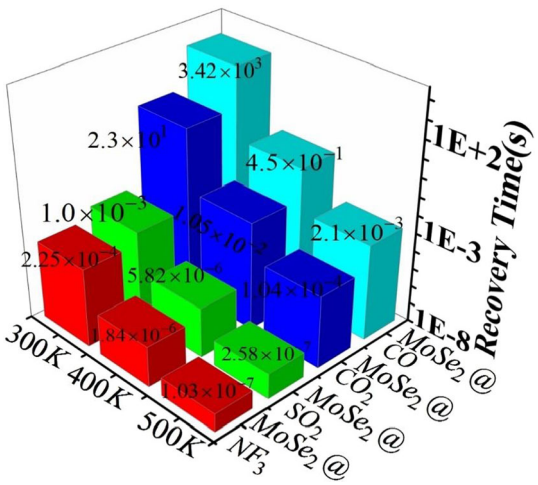

Fig. 7 Recovery time of different sensing systems

different bias voltages are applied. As opposed to the pure $MoSe_2$ monolayer, gas molecules adsorbed on the $MoSe_2$ monolayer, such as CO, CO_2, SO_2, and NF_3, showed the greatest current fluctuation with voltage. It was found that the pristine current is zero from 0 to 1 V bias and increases to 1.2 μA at 2 V. The I–V properties of the $MoSe_2$ monolayer before as well as after adsorption with the gases are shown in Fig. 9. From 0 to 1 V bias voltage, the device is in turned off condition. At 2 V bias voltage, the observed currents are 1.2 μA for pristine $MoSe_2$, 2.14 μA for CO absorbed, 2.96 μA for CO_2 absorbed, 4.06 μA for SO_2 and 5.50 μA for NF_3 absorbed. Because of the high surface-to-volume ratio in nano devices such as 2-D $MoSe_2$ monolayer devices, surface states and interface traps play a more significant role in causing current nonlinearity. Moreover, defects and variability introduced by nanoscale manufacturing can result in varying electric fields and carrier transport, which further exacerbates nonlinear behavior.

Sensitivity is explicitly defined as the relative change in current (conductance) caused by the adsorption of gas molecules in the context of a 2-D material-based sensor that detects gas molecules. This is frequently stated as a change in percentage or fraction. The formula below is used to determine the sensitivity (S) of the gases to assess how a monolayer $MoSe_2$ sensor reacts to harmful gases like CO, CO_2, SO_2, and NF_3 molecules.

$$S = \frac{|G - G_0|}{G_0} = \frac{|I - I_0|}{I_0} \tag{9}$$

where, the conductance and electric current, respectively, in the presence and absence of gas molecules are denoted by (G, G_0) and (I, I_0). Figure 10 illustrates the $MoSe_2$ monolayer sensitivity to harmful gases like CO, CO_2, SO_2, and NF_3 molecules. The $MoSe_2$ monolayer-based gas sensor for harmful gases like CO, CO_2, SO_2, and NF_3 molecules exhibits an increment in sensitivity at 1.6 V but after that sensitivity decreases. It is observed that at voltages (e.g., V = 1.6 V), the $MoSe_2$ gas sensor shows improved sensing capability.

11 Conclusion

Van der Waals corrected DFT simulations were accustomed to analyzing the adsorption behavior as well as electronic characteristics of the molecules adsorbed by the $MoSe_2$ monolayer in order to investigate its potential as a high-performance ambient temperature CO, CO_2, SO_2, and NF_3 sensor. The adsorption of these molecules on the $MoSe_2$ monolayer has been thoroughly investigated theoretically, and the modifications in the band structure (E_g), DOS, adsorption energy (E_{ads}), and recovery time have all been examined. All of the gases adsorb on the $MoSe_2$

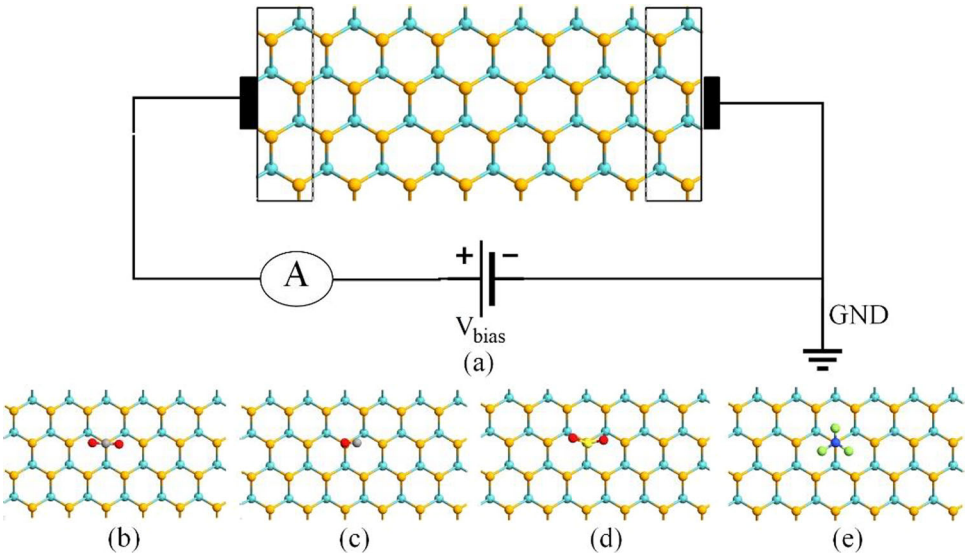

Fig. 8 **a** Circuit diagram of 2-D $MoSe_2$ monolayer, **b** $MoSe_2$@CO_2, **c** $MoSe_2$@CO, **d** $MoSe_2$@SO_2, **e** $MoSe_2$@NF_3

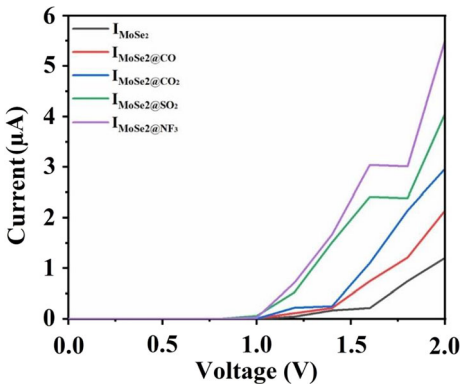

Fig. 9 IV characteristics

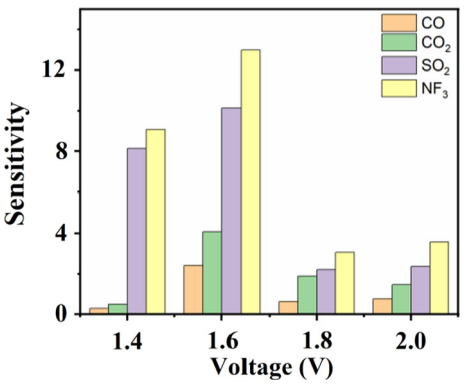

Fig. 10 Sensitivity plot of the gas sensors

single layer by the physisorption process, according to our data, which also suggests the adsorption energy follows the sequence $NF_3 > SO_2 > CO_2 > CO$. Additionally, all three gases had fast recovery times, which is a crucial result as it establishes whether or not a sensing material is worth recycling. The CO (3422.8 s) molecule has a very significant recovery time, whereas the CO_2 (23.06 s), SO_2 (1 ms), and NF_3 (0.22 ms) molecules have very low values of recovery durations. Since $MoSe_2$ has a very low recovery time, it can be used as a reusable and recyclable sensor for detecting NF_3 and SO_2. The very sensitive nature of the $MoSe_2$ monolayer is confirmed by the considerable fluctuation in its I–V properties following exposure to gas molecules. Our findings suggest that 2-D $MoSe_2$ monolayers may be employed as gas sensor materials with multi-time reusability and recyclability for several gases (CO, CO_2, SO_2, and NF_3).

Author contributions Mr. Suman Sarkar and Dr. Manash Chanda conceived of the presented idea. Mr. Sarkar developed the theory and performed the computations. Dr.Debnath and Prof. (Dr.) De verified the analytical methods. Dr. Chanda encouraged Mr. Sarkar to investigate the sensing behavior of the 2D material in depth and supervised the findings of this work. All authors discussed the results and contributed to the final manuscript.

Data availability No datasets were generated or analysed during the current study.

Declarations

Conflict of interest The authors declare no competing interests.

References

Becke AD (1993) A new mixing of Hartree-Fock and local density-functional theories. J Chem Phys 98(2):1372–1377

Bo Z, Guo X, Wei X, Yang H, Yan J, Cen K (2019) Density functional theory calculations of NO2 and H2S adsorption on the group 10 transition metal (Ni, Pd and Pt) decorated graphene. Phys E Low-Dimens Syst Nanostruct 109:156–163

Chen X, Wong CKY, Yuan CA, Zhang G (2013) Nanowire-based gas sensors. Sens Actuators B Chem 177:178–195. https://doi.org/10.1016/j.snb.2012.10.134

Cui H, Zhang X, Li Y, Chen D, Zhang Y (2019a) First-principles insight into Ni-doped InN monolayer as a noxious gases scavenger. Appl Surf Sci 494:859–866

Cui H, Zhang X, Chen D, Tang J (2019b) Pt & Pd decorated CNT as a workable media for SOF2 sensing: a DFT study. Appl Surf Sci 471:335–341

Cui H, Liu T, Zhang Y, Zhang X (2019c) Ru-InN monolayer as a gas scavenger to guard the operation status of SF 6 insulation devices: a first-principles theory. IEEE Sens J 19(13):5249–5255

Cui H, Jiang J, Gao C, Dai F, An J, Wen Z, Liu Y (2022) DFT study of Cu-modified and Cu-embedded WSe2 monolayers for cohesive adsorption of NO2, SO2, CO2, and H2S. Appl Surf Sci 583:152522

Delley B (1990) An all-electron numerical method for solving the local density functional for polyatomic molecules. J Chem Phys 92(1):508–517

Demir S, Fellah MF (2020) A DFT study on Pt doped (4, 0) SWCNT: CO adsorption and sensing. Appl Surf Sci 504:144141

Diederich F, Rubin Y, Diederich F, Rubin Y (1992) Strategien zum Aufbau molekularer und polymerer Kohlenstoffallotrope. Angew Chem 104(9):1123–1146

Flamm DL (1993) Feed gas purity and environmental concerns in plasma etching. Solid State Technol 36:43–48

Geim AK, Novoselov KS (2007) The rise of graphene. Nat Mater 6(3):183–191

Gorman D, Drewry A, Huang YL, Sames C (2003) The clinical toxicology of carbon monoxide. Toxicology 187:25–38

Grimme S (2006) Semiempirical GGA-type density functional constructed with a long-range dispersion correction. J Comput Chem 27(15):1787–1799. https://doi.org/10.1002/jcc.20495

Hoa ND, Van Quy N, Cho Y, Kim D (2009) Porous single-wall carbon nanotube films formed by in Situ arc-discharge deposition for gas sensors application. Sens Actuators B Chem 135(2):656–663

Hussein TA, Shiltagh NM, Alaarage WK, Abbas RR, Jawad RA, Nasria AH (2023) Electronic and optical properties of the BN bilayer as gas sensor for CO2, SO2, and NO2 molecules: a DFT study. Results in Chemistry. 5:100978. https://doi.org/10.1016/j.rechem.2023.100978

Kadioglu Y, Gökoálu G, Aktérk OÜ (2017) Molecular adsorption properties of CO and H_2O on Au-, Cu-, and AuxCuy-doped MoS2 monolayer. Appl Surf Sci 425:246–253. https://doi.org/10.1016/j.apsusc.2017.06.333

Kang J, Tongay S, Zhou J, Li J, Wu J (2013) Band offsets and heterostructures of two-dimensional semiconductors. Appl Phys Lett 102(1):012111

Lu P, Zhang H, Wu J (2017) Inhomogeneous radiative forcing of NF3. Atmosphere 8:17

Mulliken RS (1955) Electronic population analysis on LCAO–MO molecular wave functions. I. J Chem Phys 23:1833–1840

Nagarajan V, Chandiramouli R (2017) Adsorption studies of alcohol molecules on monolayer MoS2 nanosheet—a first-principles insights. Appl Surf Sci 413:109–117

Pearton SJ, Ren F, Wang YL, Chu BH, Chen KH, Chang CY, Lim W, Lin J, Norton DP (2010) Recent advances in wide bandgap semiconductor biological and gas sensors. Prog Mater Sci 55:1–59

Peng S, Cho K, Qi P, Dai H (2004) Ab initio study of CNT NO2 gas sensor. Chem Phys Lett 387(4–6):271–276

Sajjad M, Feng P (2014) Study the gas sensing properties of boron nitridenanosheets. Mater Res Bull 49:35–38. https://doi.org/10.1016/j.materresbull.2013.08.019

Salih E, Ayes AI (2020) CO, CO2, and SO2 detection based on functionalized graphene nanoribbons: First principles study. Physica E 123:114220. https://doi.org/10.1016/j.physe.2020.114220

Sarkar S, Debnath P, De D, Chanda M (2022) A DFT based approach to sense the SF6 decomposed gases using Ni-doped WS2 monolayer. IETE Tech Rev 40:621–631

Sarkar S, Debnath P, De D, Chanda M (2023) A DFT based approach for NO2 sensing using Vander Wall hetero monolayer. IETE J Res 2023:1–12

Sarkar S, Debnath P, Chanda M, De D (2021) DFT based approach to sense SF 6 decomposed gases (SO 2, SOF 2, SO 2 F 2) using Ni doped WS2 monolayer. In: 2021 Devices for Integrated Circuit (DevIC), pp 643–647

Shen Y, Yu M, Huang R, Cheng Q (2022) Numerical simulation of n-MoSe2/p-Si solar cells by AFORS-HET. Adv Theory Simul 5(7):2100551

Tit N, Said K, Mahmoud NM, Kouser S, Yamani ZH (2017) Ab-initio investigation of adsorption of CO and CO_2 molecules on graphene: role of intrinsic defects on gas sensing. Appl Surf Sci 394:219–230

Tsai W-T (2008) Environmental and health risk analysis of nitrogen trifluoride (NF3), a toxic and potent greenhouse gas. J Hazard Mater 159(2–3):257–263

Yamakasi AJ (2003) An overview of CO_2 mitigation options for global warming—emphasizing CO_2 sequestration options. J Chem Eng Jpn 36:361–376

Yang Q, Meng R-S, Jiang J-K, Liang Q-H, Tan C-J, Cai M, Sun X, Yang D-G, Ren T-L, Chen X-P (2016) First-principles study of sulfur dioxide sensor based on phosphorenes. IEEE Electron Device Lett 37:660–662

Yogi R, Jaiswal NK (2019) Adsorption of CO gas molecules on zigzag BN/AlN nanoribbons for nanosensor applications. Phys Lett 383:532–538

Zhang J, Liu X, Neri G, Pinna N (2016) Nanostructured materials for room-temperature gas sensors. Adv Mater 28(5):795–831

Zhang D, Wu J, Li P, Cao Y (2017) Room-temperature SO2 gas-sensing properties based on a metal-doped MoS2 nanoflower: an experimental and density functional theory investigation. J Mater Chem A 5(39):20666–20677

Zhang D, Zong X, Wu Z, Zhang Y (2018) Ultrahigh-performance impedance humidity sensor based on layer-by-layer self-assembled tin disulfide/titanium dioxide nanohybrid film. Sens Actuators B 266:52–62

Zhang YH, Wang CN, Yue LJ, Chen JL, Gong FL, Fang SM (2021) Nitrogen-doped graphene quantum dot decorated ultra-thin ZnO nanosheets for NO_2 sensing at low temperatures. Physica E 133:114807

Zhao P, Zheng J, Guo P, Jiang Z, Cao L, Wan Y (2017) Electronic and magnetic properties of re-doped single-layer MoS2: a DFT study. Comput Mater Sci 128:287–293. https://doi.org/10.1016/j.commatsci.2016.11.030

Zhao Z, Yong Y, Zhou Q, Kuang Y, Li X (2020) Gas-sensing properties of the SiC monolayer and bilayer: a density functional theory study. ACS Omega 5(21):12364–12373